Electronic Supplementary Information (ESI) Document:

Ammonia-salt solvent promotes cellulosic biomass deconstruction under ambient pretreatment conditions to enable rapid soluble sugar production at ultra-low enzyme loadings

Shishir P. S. Chundawat,[a]* Leonardo da Costa Sousa,[b] Shyamal Roy,[a,c] Zhi Yang,[d] Shashwat Gupta,[a] Ramendra Pal,[e] Chao Zhao,[a,f] Shih-Hsien Liu,[g] Loukas Petridis,[g] Hugh O' Neill,[d] Sai Venkatesh Pingali[d]

a) *Department of Chemical & Biochemical Engineering, Rutgers The State University of New Jersey, Piscataway, NJ 08854, USA. *Corresponding Author Email: shishir.chundawat@rutgers.edu*
b) *Department of Chemical Engineering & Materials Science, Michigan State University, East Lansing, MI 48824, USA.*
c) *Department of Chemical Engineering, Jadavpur University, Jadavpur, Kolkata, West Bengal 700032, India. (Current Address)*
d) *Center for Structural Molecular Biology, Oak Ridge National Laboratory, Oak Ridge, TN 37831, USA.*
e) *Department of Mechanical & Aerospace Engineering, Rutgers The State University of New Jersey, Piscataway, NJ 08854, USA.*
f) *School of Engineering, Zhejiang A&F University, Linan, Zhejiang 311300, People's Republic of China. (Current Address)*
g) *UT/ORNL Center for Molecular Biophysics, Oak Ridge National Laboratory, Oak Ridge, Tennessee 37831, USA.*

Number of Pages: 29
Number of Figures: 13
Number of Tables: 5
Number of Movies: 1

ESI Methods & Results Section:

M1. X-ray diffraction (XRD) method and data analysis

XRD was performed on a Philips X'Pert X-ray Powder Diffractometer (Malvern Panalytical Ltd., Royston, UK). CuKα radiation (wavelength = 1.5418 Å) was generated at 40 kV and 40 mA. Detector slit was set to 0.3 mm. Sample was analyzed using a coupled 2θ/θ scan type with a continuous PSD fast scan mode. The 2θ started at 3° and ended at 90° with a step size of 0.02° and time step of 3 seconds per step. Lyophilized cellulose samples (approximately 0.3 g) were placed in a rotating specimen holder ring (4 secs/revolution).

Cellulose crystallinity index (CrI), for Avicel based cellulose I and III allomorphs, was quantified based on two different methods, namely; XRD peak height and peak deconvolution methods, as highlighted elsewhere.[1,2] For the XRD peak height method, CrI was calculated from the ratio of the height of the 002 peak (I_{002}) and the height of the minimum (I_{AM}) between the 002 and 101 peaks ($CrI = 100*(I_{002}-I_{AM})/I_{002}$). The I_{002} and I_{AM} peaks for cellulose I were at 22.5° and 18.6°, while for cellulose III they were at 20.7° and 17.8°, respectively. The CrI estimated based on the peak height method for cellulose I and III controls were 84% and 79%, respectively. For the XRD peak deconvolution method, peak deconvolutions were carried out using PeakFit software (Version 4.12, Systat Software Inc, San Jose, CA) as described elsewhere.[2] For all peak deconvolutions F values are always > 15,000 while R-squares > 0.99. For cellulose I and all relevant ammonia:ammonium thiocyanate or A:At treated cellulose-I samples, five crystalline peaks (at 14.76°, 16.38°, 20.53°, 22.40°, and 34.34°) and one amorphous peak (21.5°) were deconvoluted and fitted to the original XRD spectra. For cellulose III and relevant A:At treated cellulose-III samples, six crystalline peaks (at 11.65°, 17.1°, 20.62°, 28.21°, 34.60°, and 35.95°) and one amorphous peak (21.5°) were deconvoluted and fitted to the original spectra. CrI based on peak deconvolution method was estimated by taking the percent ratio of the crystalline peak area (AC) to the total area (AT) of all deconvoluted peaks ($CrI= 100*AC/AT$). The CrI for cellulose I and III controls were 66% and 58%, respectively. The average crystallite size was next estimated based on the width of the most intense deconvoluted crystalline peak (e.g., 002 reflection) at half height using the Scherrer equation ($D = 57.3K\lambda/(\beta \cos(\theta))$).[3] Where; D is the average dimension of the crystallite area measured vertically to the corresponding reflecting lattice plane, K is the form factor constant equal to 0.89, λ is the wavelength of the incident X–ray equal to 1.5418 Å, 57.3 is the conversion factor for degrees to radians, θ is the Bragg diffraction angle of X–rays on the plane under consideration, and β is the full width half maximum of the X–ray peak corresponding to the 002 peak. Average size of the Avicel derived cellulose I and III control crystallites corresponding to the respective deconvoluted 002 peaks were 5.1 and 4.2 nm, respectively. Note that for 6 h and 24 h A:At treated cellulose III, only three peaks (at ~22°, ~28°, ~34°) could be deconvoluted and fitted to the highly amorphous XRD spectra. Therefore, crystallite size analysis for 6 h and 24 h A:At treated cellulose III was performed using the dominant broad amorphous peak at ~22° for sake of comparison with other treated samples.

M2. Scanning Electron Microscopy (SEM) analysis

SEM analyses on all lyophilized cellulose samples were performed using a Zeiss Sigma field emission SEM (Carl Zeiss Microscopy, Jena, Germany) equipped with x-ray energy dispersive spectrometry (EDS) capabilities with an Oxford INCA energy 250 microanalysis system (Oxford

Instruments NanoAnalysis, MA, USA). Electrons were generated using a ZrO-W Schottky field emission gun source. All samples were mounted on aluminum stubs using carbon tape and they were coated with a 5 nm conductive film of gold using a sputter coater. The electron beam was set at 2.0 keV to prevent electron beam induced damage to the specimens and analyses were performed at different magnifications to obtain representative imaging data.

M3. Impact of of A:At treated recovered cellulose lyophilization on cellulase activity

A:At treated cellulose I and cellulose III generated after treatment for varying treatment durations were lyophilized for XRD analysis. Therefore, we also performed enzymatic hydrolysis on all lyophilized cellulose samples at a fixed enzyme loading (5 mg Cellic C.Tec2/g glucan) to study impact of lyophilization on cellulase activity. Briefly, all lyophilized pretreated cellulose samples were subjected to enzymatic hydrolysis at 2.5% glucan loading in 10 ml reaction volume using 15 ml glass vials as described before,[1] based on the original NREL protocols.[4] In all assays, final reaction volume pH 4.8 was achieved using 50 mM sodium citrate buffer and sodium azide was added to prevent any microbial growth (0.1% w/v final concentration). Vials were incubated at 50 °C in an orbital shaking incubator set at 150 RPM (New Brunswick, Innova 44, Enfield, CT) for desired saccharification time (24, 72 h). The hydrolysate supernatants were analyzed for total reducing sugar concentrations using the standard dinitrosalicylic acid (DNS) colorimetric assay or glucose/xylose based enzymatic assay kits as reported earlier.[5]

M4. Corn stover A:At pretreatment mass balance and compositional analysis methods

The corn stover used here was generously provided by the Great Lakes Bioenergy Research Center (GLBRC). The moisture content of the milled corn stover was approximately 9% (total weight basis) and was used as is for A:At pretreatment without any pre-activation of the cellulose. Briefly, corn stover was pretreated directly using a ~27:73% (dry weight basis or dwb) ammonia-ammonium thiocyanate solution as described below. A:At solution was prepared as described previously.[6,7] For all ex-situ ammonia-salt pretreatments, add 4 g (twb) of corn stover along with ~100 ml of ammonia-salt solution in a 500 mL stoppered glass bottle and mix slurry using a magnetic stirrer at 500 rpm for desired pretreatment time (24 h) at room temperature. At the desired sampling time after 24 h, add 100 mL of ethanol (100%) as anti-solvent to precipitate solubilized polysaccharides out of solution. Filter and wash the recovered solid precipitate with excess ethanol (50:1, v/w), followed by five washes with 1:1 ethanol-acetone (20:1, v/w) to remove any traces of residual ammonia-salt. Store all treated biomass samples in a never-dried state, soaked in 100% ethanol, at 4 °C prior to usage.

Untreated CS and A:At treated CS solids were subjected to compositional analysis using a slightly modified NREL/TP-510-42618 and NREL/TP-510-42620 protocols, where biomass was not extracted with water/ethanol prior to acid hydrolysis and neutralized sugar hydrolysates were analyzed using a suitable glucose/xylose enzyme assay kits to estimate sugar concentrations instead.[5] Mass balances on total glucan, xylan, and lignin (acid soluble and acid insoluble) were performed before and after the A:At pretreatment. Untreated corn stover contained approximately 40.6±0.8% glucan, 22.4±2.9% xylan, 21.5±2.9% Klason lignin, and 1.4±0.9% acid-soluble lignin based on a dry weight basis. While, A:At treated corn stover contained approximately 48.6±7.5% glucan, 23.5±0.0% xylan, 3.6±1.9% Klason lignin, and 1.2±0.4% acid-soluble lignin based on a dry weight basis. Here, all mass balance and compositional analysis experiments were done in two replicate batches conducted on two separate days each and the relevant mean values and

corresponding standard deviations are reported here. The A:At CS extractives composition was indirectly estimated based on the untreated CS and A:At CS substrate composition as well as the ~85% solids mass recovery values.

Please note that since we are currently interested in showing proof-of-concept of how an A:At type pretreatment process would actually work on real-world relevant lignocellulosic biomass, we monitored the changes in composition of corn stover for key representative monocot grasses cell wall components, namely cellulose, xylan, and acid-insoluble (Klason)/acid-soluble lignin. We did not attempt to perform a detailed composition analysis of all expected plant cell wall components, therefore the mass balance currently only accounts for ~77-85% of total dry weight of starting biomass material. The remaining 15-23% of the starting material will likely have significant contributions from arabinan (~3-5%), mannan (~1-2%), galactans (~2-3%), proteins (~3-5%), acetyls (~3-5%), uronic acids (~3-5%), and/or non-structural components like sucrose (~1-2%) and ash often reported in monocot grasses like stover. Templeton and co-workers have performed detailed analysis of different compositional analysis methods and systematically studied the overall variance in corn stover composition,[8,9] providing details on other likely cell wall components not analyzed currently. Future work will focus on investigating the detailed composition of corn stover as a function of various A:At pretreatment conditions at larger scale for increased mass balance accuracy and also identify the chemical/structural changes likely taking place during pretreatment analogous to work reported for AFEX/EA pretreatment.[10–12]

M5. Molecular dynamics simulations of model cellulose chain in A:At solvent system

Atomistic Model. The model cellulose chain used for all MD simulations was cellohexaose, which contains six β1-4 linked β-D-glucose monomers. Two solvent environments of cellohexaose were examined: 1) cellohexaose:ammonia:ammonium thiocyanate (A:At) with a relative weight ratio of 1.2:27:73, respectively; and 2) cellohexaose in water. The molecules were packed in a cubic box with a side length of 51 Å using Packmol.[13] To ensure our findings do not depend on one initial configuration, we performed three independent simulations (i.e., instances) with different initial structures and initial velocity distributions.

Force Field. CHARMM36 force field parameters were used for cellohexaose and ammonia,[14,15] and the TIP3P model[16] was used for water. For ammonium cation (NH_4^+), its force field parameters were derived from methylammonium ($CH_3NH_3^+$) in CHARMM,[14,15,17] and are shown in Table S2. For thiocyanate anion (SCN^-), we obtained its force field parameters using Force Field Toolkit (ffTK)[18] implemented in VMD[19] in combination with Gaussian09.[20] We then optimized its Lennard-Jones potential until the simulation-derived solvation free energy (ΔG_{sol}) was in good agreement with experiment.[21] Table S3 shows the optimized force field parameters for SCN^- employed in this work. To validate the parameters for NH_4^+ and SCN^-, we calculated their ΔG_{sol} from the MD simulations and compared them to experiment (Table S4).

MD Simulations. We employed the GROMACS simulation code.[22] For each of the three instances, we first performed energy minimization followed by 5 ns of equilibration and 110 ns of production in an NPT ensemble with a time step of 1 fs at 293 K and 0.55 bar to model the vapor pressure of ammonia in a closed container.[23] 300 K and 1 bar were applied to cellohexaose in water. We used a v-rescale thermostat[24] with 0.1 ps as the time constant for coupling to maintain constant temperature, and Berendsen[25] and Parrinello-Rahman[26] barostats with 1 ps as the time constant for

coupling to maintain constant pressure for equilibration and production, respectively. The isothermal compressibility for pressure coupling was 0.00015 bar^{-1}, which applies to liquid ammonia at 293 K.[27] We used Verlet cutoff-scheme, fast smooth particlemesh Ewald (PME)[28] electrostatics and linear constraint solver (LINCS)[29] algorithm on hydrogen-containing bonds. The instantaneous energies and configurations were saved every 10 ps. The last 100 ns for each of the three instances were used for analysis, and all the calculated values represent averages over the three instances. Figure S5 shows a snapshot of the equilibrated cellohexaose in A:At solvent. Movie S1 shows how the structure of cellohexaose changes in A:At solvent along MD simulation time and can be downloaded on the RSC website.

Conformations of the C6-Hydroxymethyl Group. We examined the conformations of the C6-hydroxymethyl group of cellohexaose in A:At and in water, excluding the two glucose monomers at chain ends. We analyzed the probability distribution of the dihedral angle ϕ of O5-C5-C6-O6 (Figure S6). ϕ = -60º, 60º, and -180º correspond to Gauche-Gauche (GG), Gauche-Trans (GT), and Trans-Gauche (TG) conformations.[30] We also obtained the relative populations of these conformations by calculating the area under each peak. The relative populations of GG:GT:TG in A:At and water are 0.35:0.48:0.17 and 0.47:0.45:0.08, respectively. Our results show that GG and GT conformations dominate in water, in agreement with a previous study.[30] Compared to water, there is a smaller GG population and a larger GT in A:At.

Cellohexaose - A:At Interactions. We resolved molecular interactions of cellohexaose with A:At solvent by calculating the radial distribution function g(r), a measure of local concentration of target species as a function of distance r from reference species,[31] between cellulose oxygen atoms that participate in the intra-chain hydrogen bonding in cellulose crystal structure.[32] Figures S7-S9 show that O2, O6, and O3 atoms interact much more strongly with ammonium cations, evidenced by the height of the first peak, as compared with thiocyanate anions and ammonia. In Figure S10, the interactions between O5 atoms and ammonium cations at r ~ 2.9 Å are still stronger than thiocyanate anions and ammonia, but its strength g(r) is much less than the other oxygen atoms in cellohexaose (Figure S11). This is likely to be attributed to the hydrogen bonding between O5 and O3 atoms.

Hydrogen Bonding Analysis. Table S5 shows that the hydrogen bonding between O2, O6, and O3 hydroxyl groups and nitrogen atoms of ammonium cations is significantly greater than thiocyanate cations and ammonia, and that O5 atoms have much weaker hydrogen bonding with ammonium cations as compared with other oxygen atoms. These hydrogen-bond findings are consistent with the g(r) results. We also see that 98% of the intra-chain O2-O6 hydrogen bonding is disrupted in A:At solvent, while only 43% of O3-O5 hydrogen bonding is disrupted. Since O3-O5 is not mostly disrupted in A:At solvent, the cellohexaose is unlikely to fold on itself and form globular shapes. A modification in formulation of A:At solvent may be required in future work to achieve globular cellulose chains as published in a recent study that used dimethyl sulfoxide to assist with cellulose dissolution in 1-ethyl-3-methylimidazoium acetate.[33]

A:At Solvent Interactions. Figure S12 shows that the interaction between ammonium cations (NH_4^+) and ammonia (NH_3) is much stronger than the other two solvent-solvent pairs. This suggests that NH_4^+-NH_3 clusters may occur in A:At solvent, which agrees with our hypothesis in experiment.

M6. Comment on viscosity of A:At and cellulose-A:At based solvent systems

Previous work has shown than ammonia based pretreatments like AFEX or EA do not significantly change cellulose degree of polymerization (DP) since cellulose polymer chain glycosidic bonds are mostly stable under AFEX-like treatment conditions at temperatures between 90-130 °C.[34] Other alkaline-catalyzed (i.e., NaOH based) cleavage reactions of cellulose glycosidic linkages to reduce cellulose DP are also virtually non-existent at room temperature.[35] This is largely because base-catalyzed cleavage of glycosidic bonds is highly sensitive to temperature. This is further clear when comparing kinetic data of the peeling-off reactions with those of alkaline hydrolysis reactions, it is obvious that alkaline hydrolysis of glycosidic bonds is a relatively slow process even at higher temperatures.[36,37] For example, Sarkanen and co-workers determined that at room temperature (25 °C), the rate constant of glycosidic bond cleavage is about 7 orders of magnitude lower than the rate observed at temperatures exceeding 150 °C.[35] Even though such reactions only become relevant during alkaline pulping or ammonia-based treatments of cellulose at temperatures exceeding 150 °C, the extent of glycosidic bond cleavage even under these extreme conditions can be marginal compared to acid-catalyzed glycosidic bond cleavage reactions. Furthermore, even any cellulose degradation which is mostly driven by reducing-end specific secondary peeling-off type reactions that do not change cellulose DP significantly since these reactions that could reduce DP are often terminated by competing stopping-type reactions. Lastly, considering that ammonia is also a weaker alkali than sodium hydroxide, it is expected that cellulose DP will also not change significantly during anhydrous ammonia-based treatments at temperatures close to 25 °C. Similarly at room temperature/pressure, A:At type solvents have also been shown to not alter cellulose DP based on the near-constant viscosity observed for cellulose-A:At solutions at 25 °C.[7] Hudson and Cuculo (1980) showed that no degradation in cellulose DP can be inferred based on the near constant viscosity of the cellulose-A:At solution at room temperature even after 24 hours. A ^{13}C-NMR study further validated that no cleavage of the glycosidic bonds was seen to take place for cellulose in the A:At solvent system.[38]

Therefore, since there was no significant change in cellulose DP or solution viscosity reported by Cuculo and co-workers for cellulose-A:At solution once the cellulose is fully dissolved in the A:At solvent, we did not attempt to monitor the viscosity change of our A:At-cellulose solutions once cellulose was full dissolved. Hudson and Cuculo (1983) also showed that the kinematic viscosity of typical A:At solutions ranged between 2-5 centistokes (cSt) at temperatures ranging between 15-35 °C at zero shear rate.[7,39] The kinematic viscosity of A:At solution alone of comparable composition, to what was reported in our current study, at 25 °C is ~3 centistokes at zero shear rate. Based on these published reports, the dynamic viscosity of equivalent A:At solution alone is therefore expected to be around 0.003 Pascal second (i.e., assuming A:At solvent density ~0.99 g/ml at 25 °C). For cellulose-A:At solutions (at ~0.02-0.2 wt% cellulose concentration), Cuculo and co-workers (Hudson 1980 and Hudson 1983) determined the relative viscosity of cellulose-A:At solutions with respect to the solvent alone at 25 °C to range between 1.2-2 for low DP cellulose samples most closely equivalent to Avicel used in our study.[7,39] We expect a similar fold change increase in the relative viscosity of the cellulose-A:At solutions once either cellulose I or III allomorphs is fully dissolved into solution. Since the concentration of cellulose used in our *ex-situ*/*in-situ* pretreatment studies were slightly higher (~2-to-5 w/v% cellulose in A:At solution), we expect the fold-change in relative viscosity to be greater than 2-fold once cellulose is fully dissolved in solution. Future work is needed to explore if there is any difference in viscosity of cellulose-A:At solutions for cellulose I versus III, though unlikely, once the cellulose is fully

dissolved in solution in either case. However, based on the SANS analysis (Table 2), cellulose III and cellulose I dissolved in A:At solution after 4 h and 72 h, respectively, have comparable structural properties. This suggests that once cellulose is fully dissolved into A:At solution the starting cellulose allomorph type will likely have limited effect, if at all any difference, on the final cellulose solution viscosity.

Furthermore, please note that the dynamic viscosity of the A:At solution alone and equivalent concentration cellulose-A:At solution is nearly 2-3 orders of magnitude lower than the viscosity of commonly reported ionic liquids (IL; e.g., 1-ethyl-3-methylimidazolium acetate) and relevant cellulose-IL solutions under comparable dissolution conditions (e.g., dissolution temperature, cellulose concentration) and cellulose properties (e.g., cellulose DP and initial crystallinity).[40] This highlights that A:At is a better low viscosity solvent for cellulose dissolution at room temperature compared to conventional ILs like 1-ethyl-3-methylimidazolium acetate that have been reported for cellulose pretreatment at process relevant biomass loading conditions.

ESI Tables and Figures:

Table S1. XRD crystallinity index (using Segal Method) and cellulose 002 equatorial reflection deconvoluted peak crystallite size (using Scherrer Method) for Avicel PH-101 cellulose-I, cellulose-III (CIII; bottom), and corresponding A:At treated samples is tabulated here. All A:At sample treatment time is provided on sample type labels along with identifier C1 (cellulose I) or C3 (cellulose III) to indicated source of starting material used for A:At treatment. All A:At treated samples were lyophilized prior to XRD analysis and data was analyzed as discussed in the ESI methods section. Note that the non-lyophilized samples were used to conduct enzymatic hydrolysis at 0.5 mg C. Tec2 enzyme/g glucan loading for 24 h saccharification time period and the hydrolysis results as a function of cellulose crystallite size reported in table below were also plotted as seen in Figure 2A.

Sample Type	%CrI (Segal)	Crystallite size (nm)
C3 control	79	4.2
AAt-C3-1 h	49	2.0
AAt-C3-3 h	48	1.9
AAt-C3-6 h	40	1.5
AAt-C3-24 h	53	1.7
Sample Type	**%CrI (Segal)**	**Crystallite size (nm)**
C1 control	84	5.1
AAt-C1-1 h	80	4.9
AAt-C1-3 h	80	5.1
AAt-C1-6 h	80	4.8
AAt-C1-24 h	79	4.3

Table S2. Force field parameters for NH_4^+ used in this work. The notations follow the convention of CHARMM,[17] and L-J stands for Lennard-Jones.

Species		Parameter	Value
N	charge	q [C]	-0.32
	L-J	ε [kcal/mol]	-0.20
		$R_{min}/2$ [Å]	1.85
H	charge	q [C]	0.33
	L-J	ε [kcal/mol]	-0.046
		$R_{min}/2$ [Å]	0.225
N-H	bonds	K_b [kcal/mol/Å^2]	403.00
		b_0 [Å]	1.04
H-N-H	angles	K_θ [kcal/mol/rad^2]	44.00
		θ_0 [deg]	109.50

Table S3. Force field parameters for SCN^- used in this work. The notations follow the convention of CHARMM,[17] and L-J stands for Lennard-Jones.

Species		Parameter	Value
S	charge	q [C]	-0.876
	L-J	ε [kcal/mol]	-0.35
		$R_{min}/2$ [Å]	2.75
C	charge	q [C]	0.071
	L-J	ε [kcal/mol]	-0.18
		$R_{min}/2$ [Å]	1.87
N	charge	q [C]	-0.195
	L-J	ε [kcal/mol]	-0.18
		$R_{min}/2$ [Å]	1.79
S-C	bonds	K_b [kcal/mol/Å^2]	314.639
		b_0 [Å]	1.666
C-N	bonds	K_b [kcal/mol/Å^2]	922.829
		b_0 [Å]	1.198
S-C-N	angles	K_θ [kcal/mol/rad^2]	3.316
		θ_0 [deg]	179.990

Table S4. Comparison between MD simulations and experiments for ΔG_{sol} [kJ/mol] of NH_4^+ and SCN^-. ΔG_{sol} was calculated following the procedures published previously.[31]

Component	MD simulations	Experiment[21]	Error
NH_4^+	-289.59 ± 0.06	-285	2%
SCN^-	-290.98 ± 0.23	-280	4%

Table S5. Hydrogen bonding analysis on cellohexaose-A:At solvent and intra-cellohexaose in A:At solvent and crystal structure. Donors are OH or NH groups, and acceptors are nitrogen or oxygen atoms. A^+, T^-, and A correspond to ammonium cation, thiocyanate anion, and ammonia, respectively. The disruption % is the difference in hydrogen bond number between crystal structure and A:At solvent divided by the number in crystal structure.

Donor-Acceptor	Hydrogen bond # in A:At solvent	Hydrogen bond # in crystal structure	Disruption % in A:At solvent
O2-NA^+	2.013 ± 0.006		
O2-NT^-	0.687 ± 0.004		
O2-NA	1.030 ± 0.006		
O6-NA^+	2.947 ± 0.006		
O6-NT^-	0.572 ± 0.004		
O6-NA	1.020 ± 0.006		
O3-NA^+	2.620 ± 0.007		
O3-NT^-	0.272 ± 0.003		
O3-NA	0.957 ± 0.005		
NA^+-O5	0.143 ± 0.002		
NA-O5	0.252 ± 0.003		
O3-O5	2.855 ± 0.006	5	43
O2-O6	0.083 ± 0.002	5	98
O6-O2	0.485 ± 0.004		

Figure S1. Representative SEM images of controls and 24 h A:At treated cellulose samples at 3000X and 500X magnifications. All samples were lyophilized prior to SEM imaging.

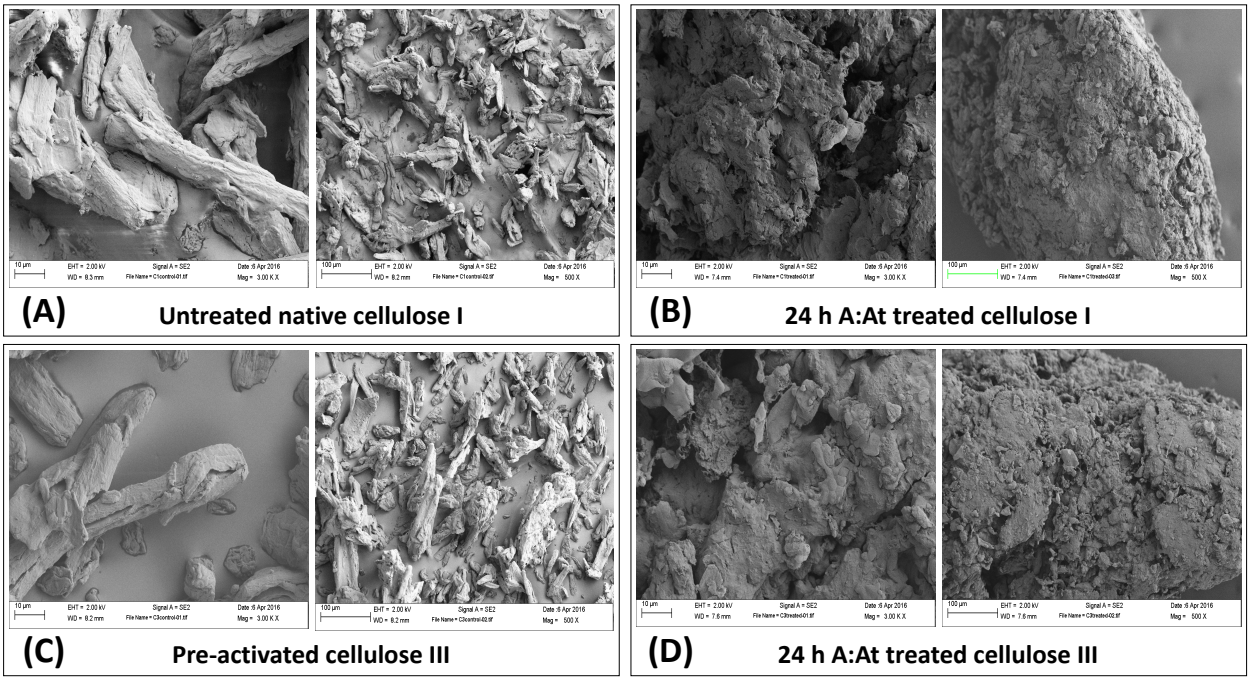

Figure S2. Representative XRD raw data (in blue) and corresponding peak deconvolution fitted spectra (in yellow) for Avicel PH-101 cellulose-I (CI; top) and cellulose-III (CIII; bottom) controls is shown here. The deconvoluted gaussian peaks for each fitted XRD spectra is shown immediately below in each XRD plot. Note that y-axis units here are XRD spectra intensity counts while x-axis units are the 2θ Bragg's scattering angle.

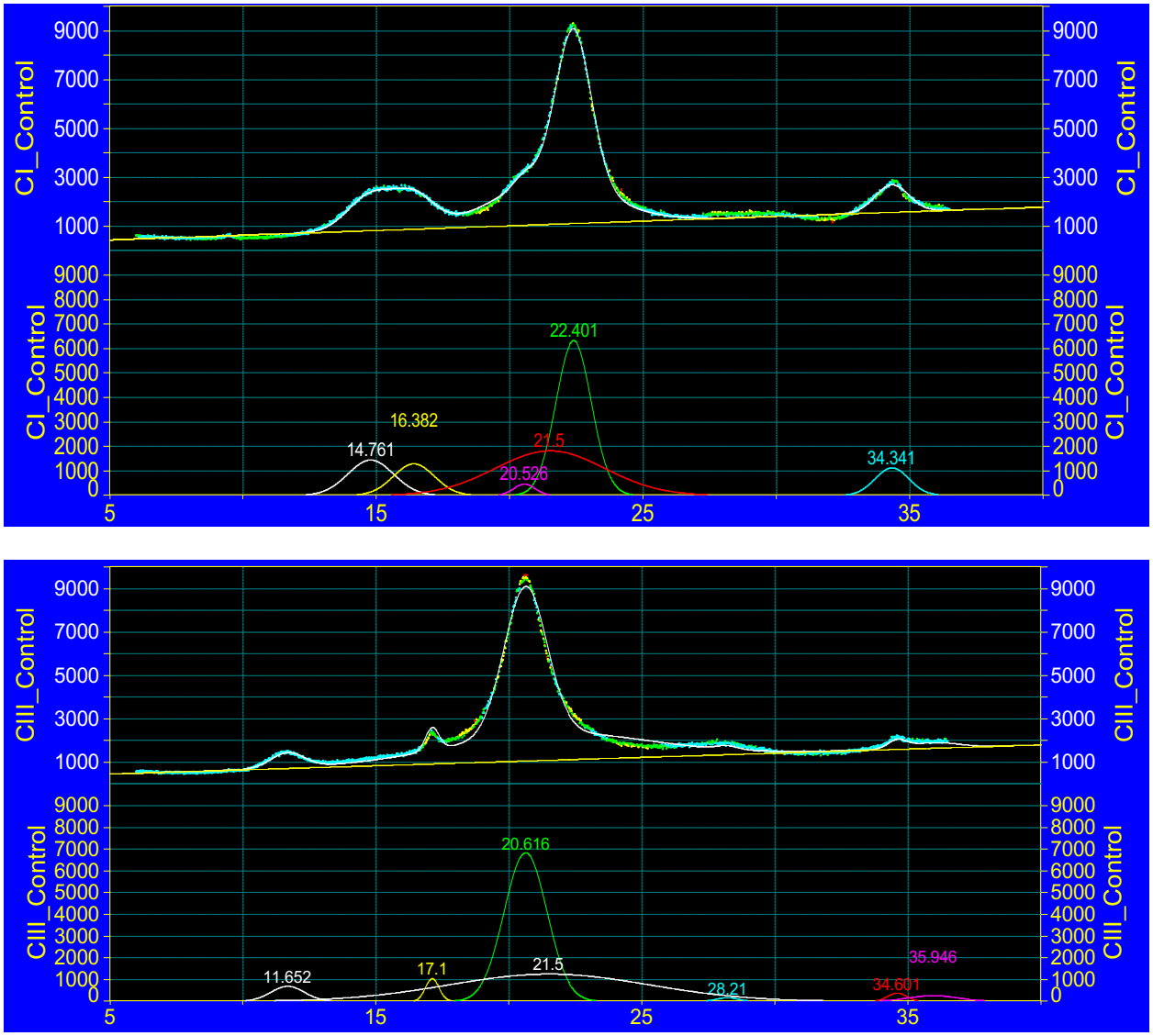

Figure S3. Impact of A:At pretreated cellulose lyophilization on enzymatic hydrolysis conversion yields, after 24 and 72 h, obtained for both controls (cellulose I or cellulose III) and respective A:At treated cellulose samples. All A:At sample treatment time is provided on the x-axis labels along with identifier CI (cellulose I) or CIII (cellulose III) to indicated source of starting material used for A:At treatment. All A:At treated samples were lyophilized prior to saccharification.

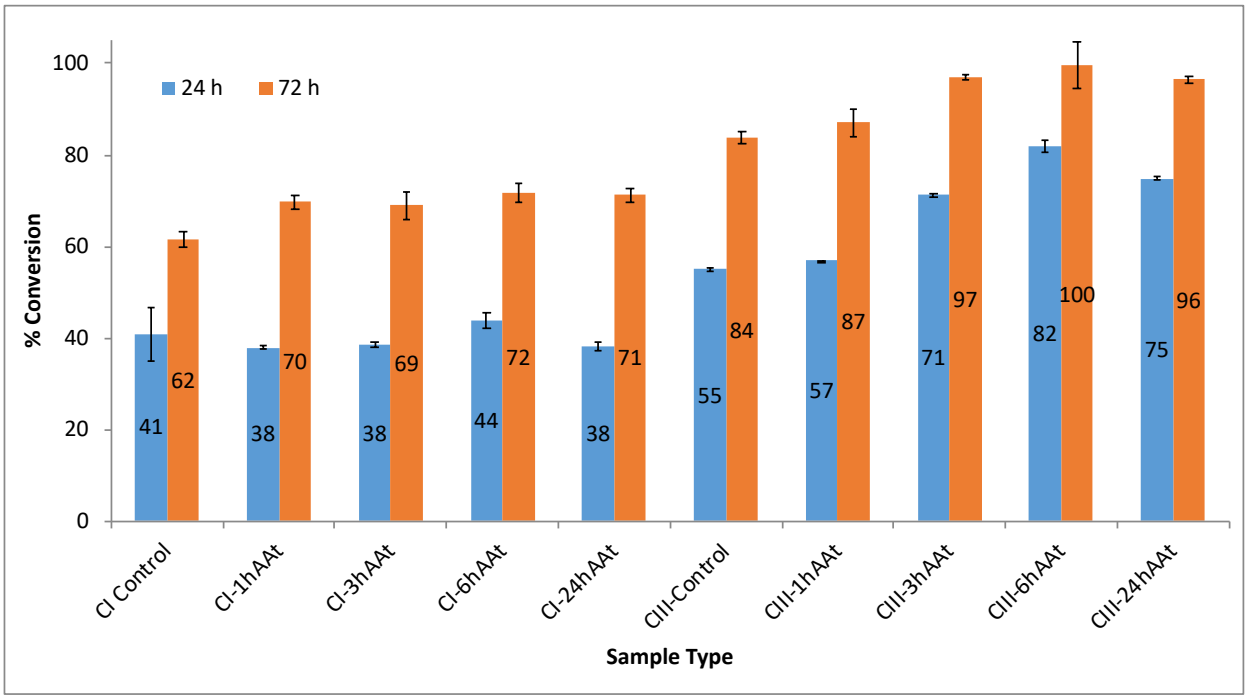

Figure S4. Small-angle neutron scattering (SANS) plot profiles for replicate sample runs are highly reproducible, as illustrated below. Here, S1 (in red below) vs. S2 (in blue above) are replicate 24 h ex-situ A:At treated cellulose III samples recovered and suspended in D_2O prior to SANS analysis.

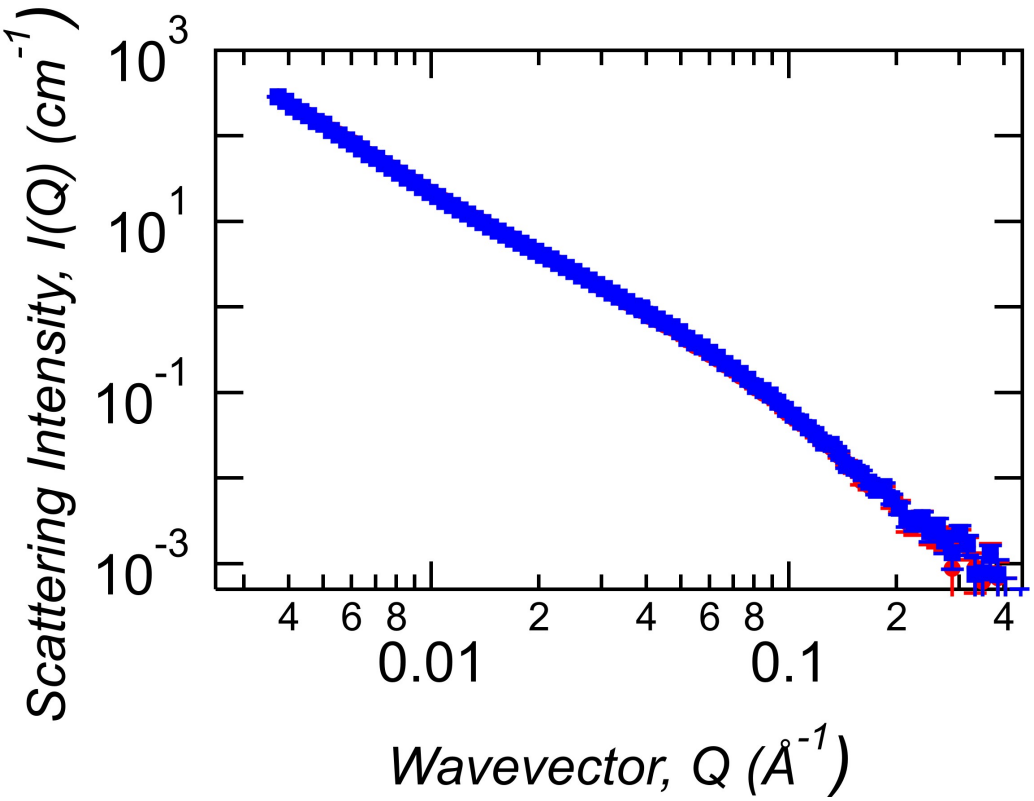

Figure S5. Equilibrated cellohexaose atomistic configurations in A:At solvent within 5 Å of cellohexaose at 293 K and 0.55 bar. Cellohexaose is shown in green, ammonia and ammonium cations are shown in blue, and thiocyanate anions are shown in magenta.

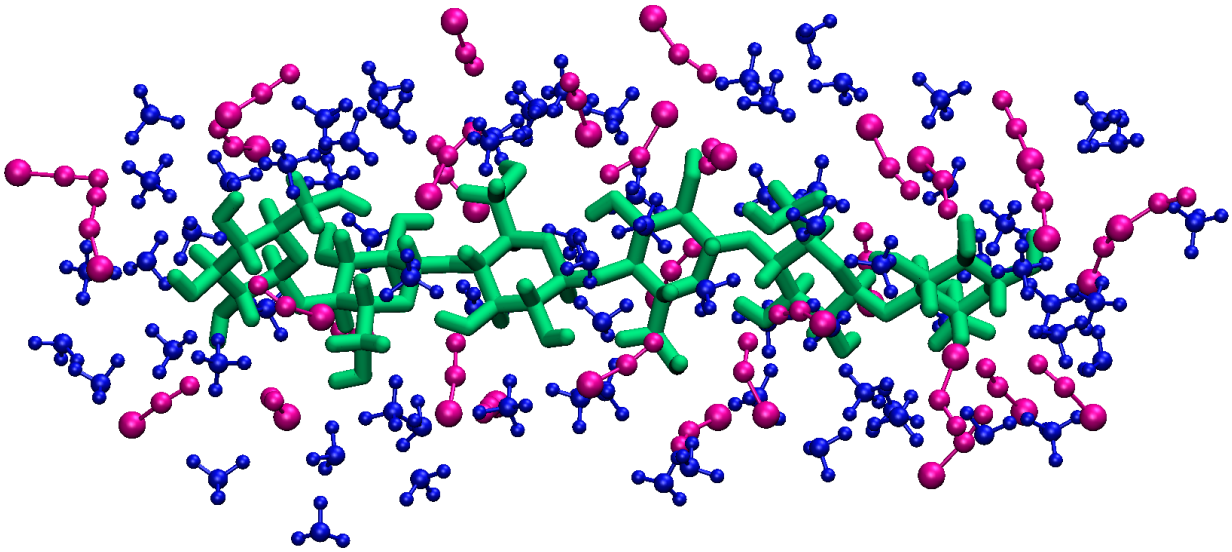

Figure S6. Probability distribution P(ϕ) with standard error bars of the dihedral angle ϕ of O5-C5-C6-O6, which determines the conformation (GG, GT, or TG) of the C6-hydroxymethyl groups, for cellohexaose in A:At or water.

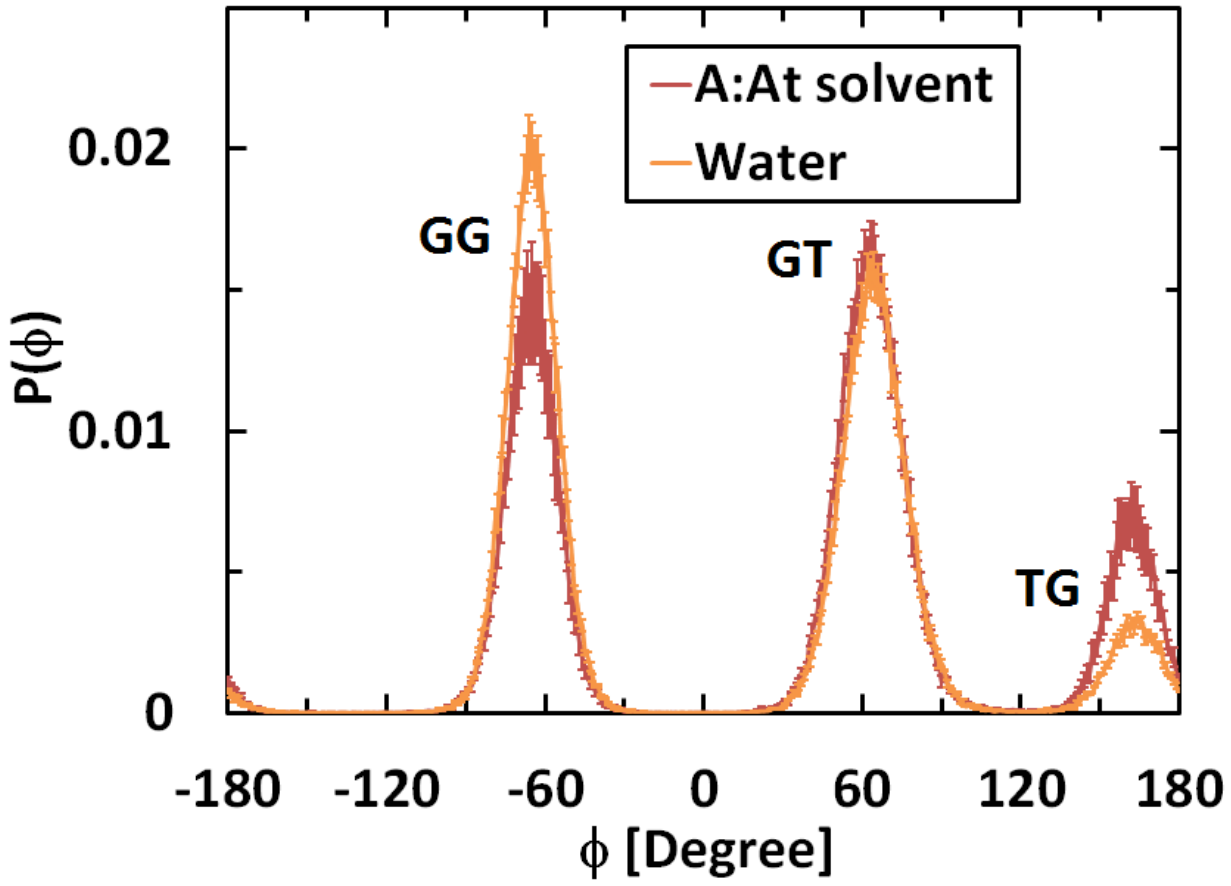

Figure S7. Radial distribution function g(r) between O2 atoms (reference) of cellohexaose and N atoms (target) of A:At solvent with standard error bars. A^+ is ammonium cation, T^- is thiocyanate anion, and A is ammonia.

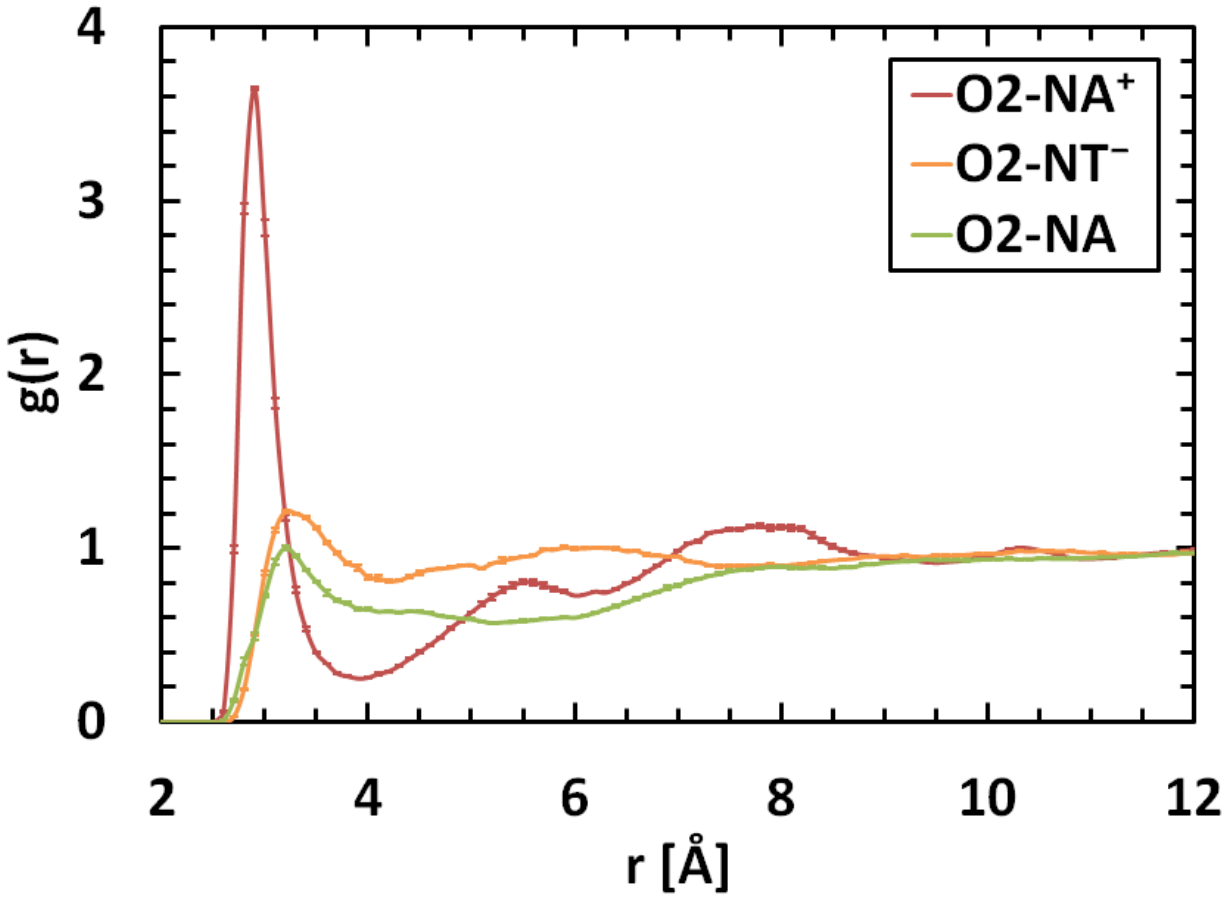

Figure S8. Radial distribution function g(r) between O6 atoms (reference) of cellohexaose and N atoms (target) of A:At solvent with standard error bars. A^+ is ammonium cation, T^- is thiocyanate anion, and A is ammonia.

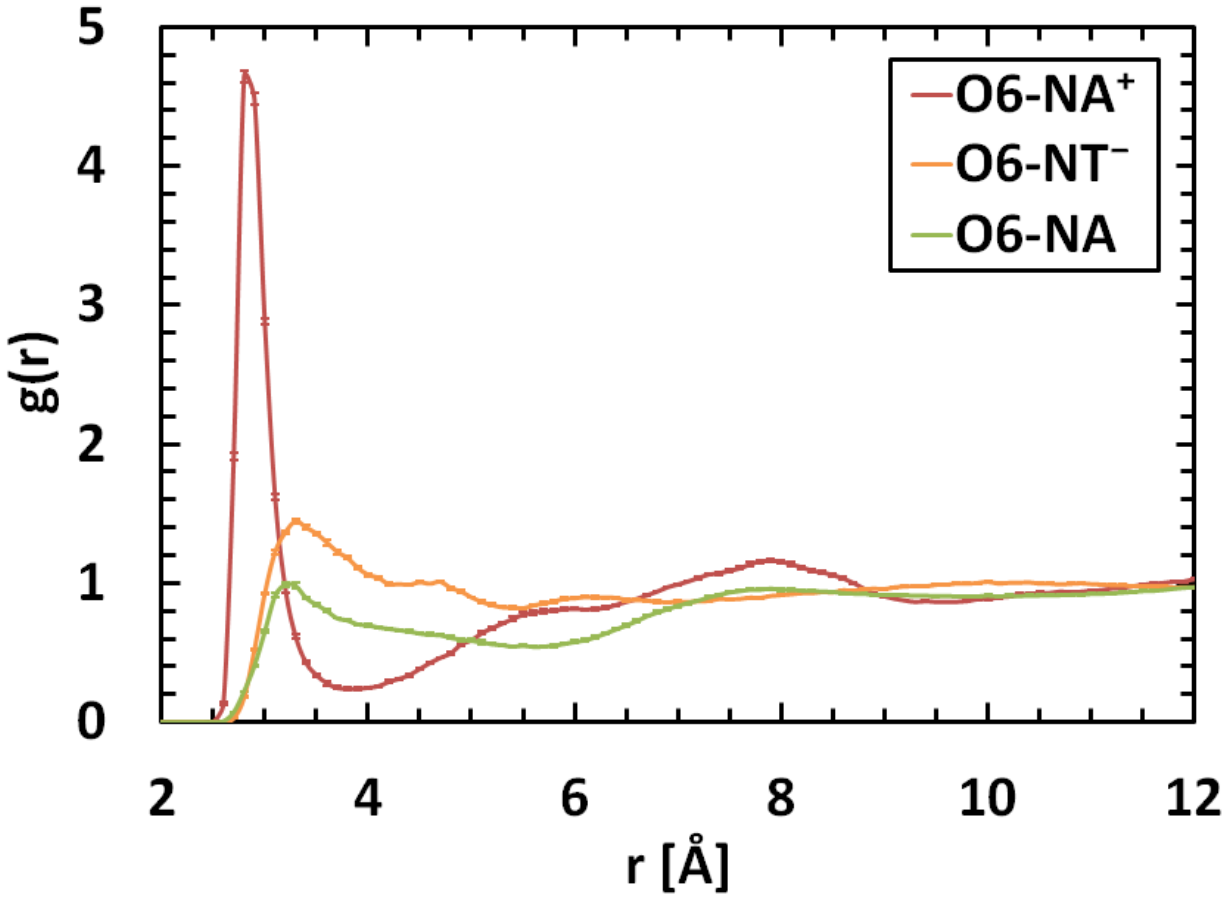

Figure S9. Radial distribution function g(r) between O3 atoms (reference) of cellohexaose and N atoms (target) of A:At solvent with standard error bars. A^+ is ammonium cation, T^- is thiocyanate anion, and A is ammonia.

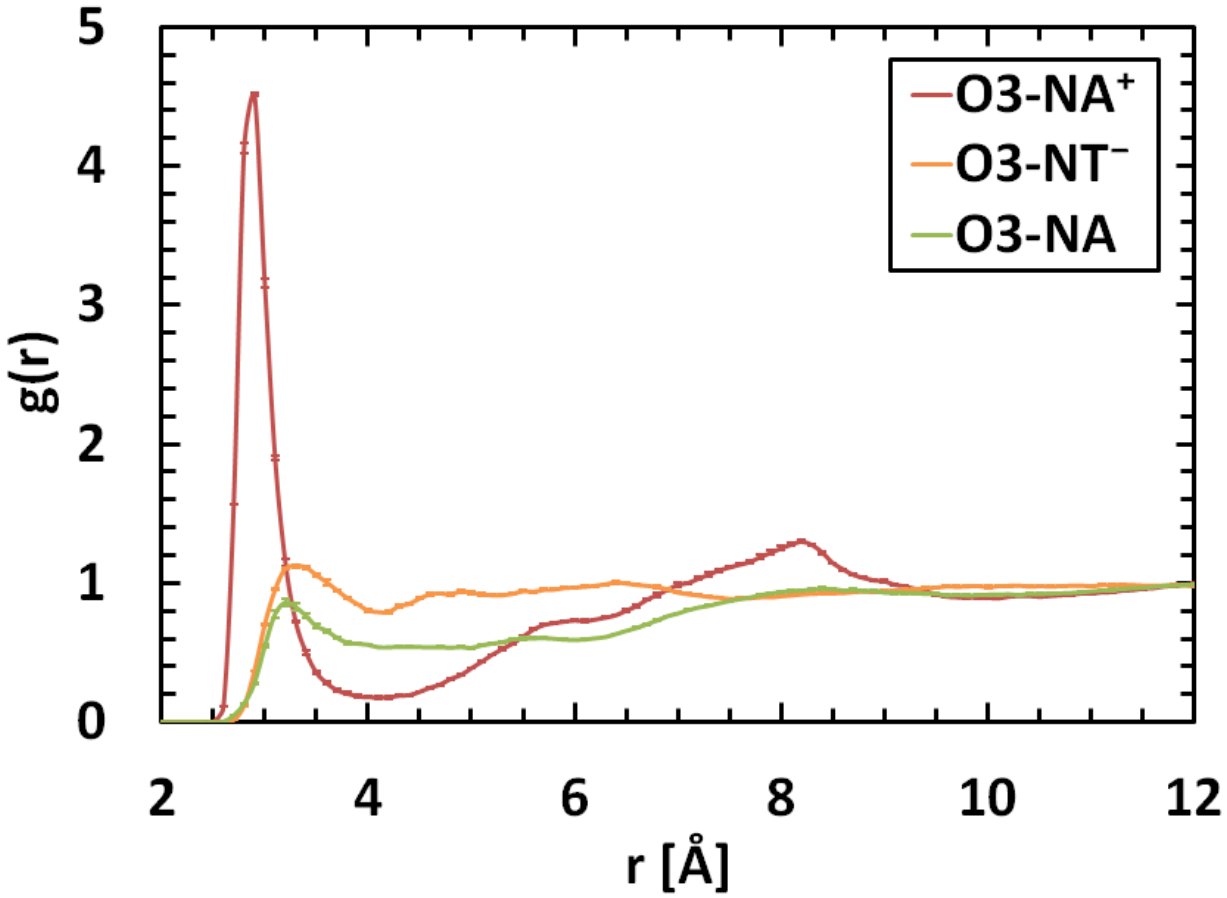

Figure S10. Radial distribution function g(r) between O5 atoms (reference) of cellohexaose and N atoms (target) of A:At solvent with standard error bars. A^+ is ammonium cation, T^- is thiocyanate anion, and A is ammonia.

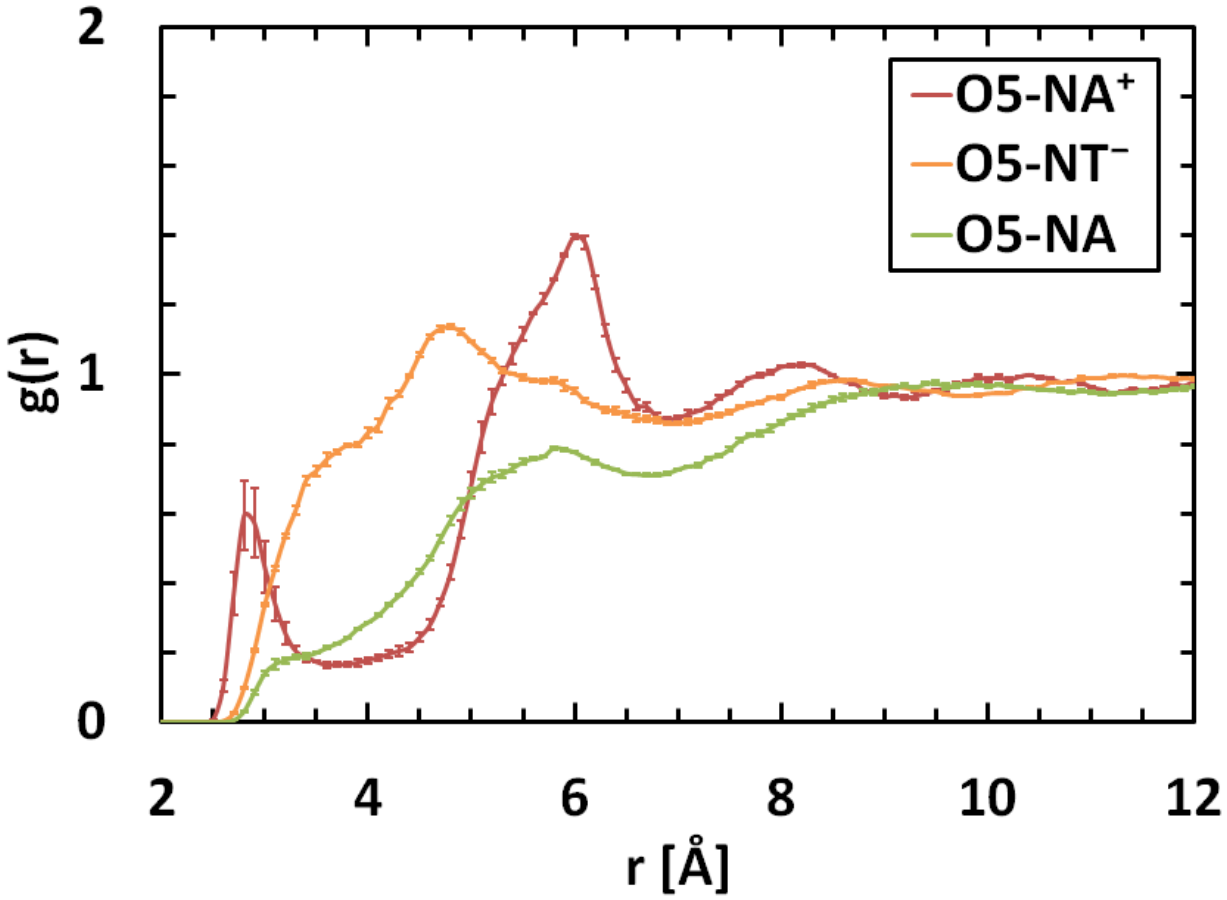

Figure S11. Radial distribution function g(r) between O atoms (reference) of cellohexaose and N atoms (target) of ammonium cation (A^+) with standard error bars.

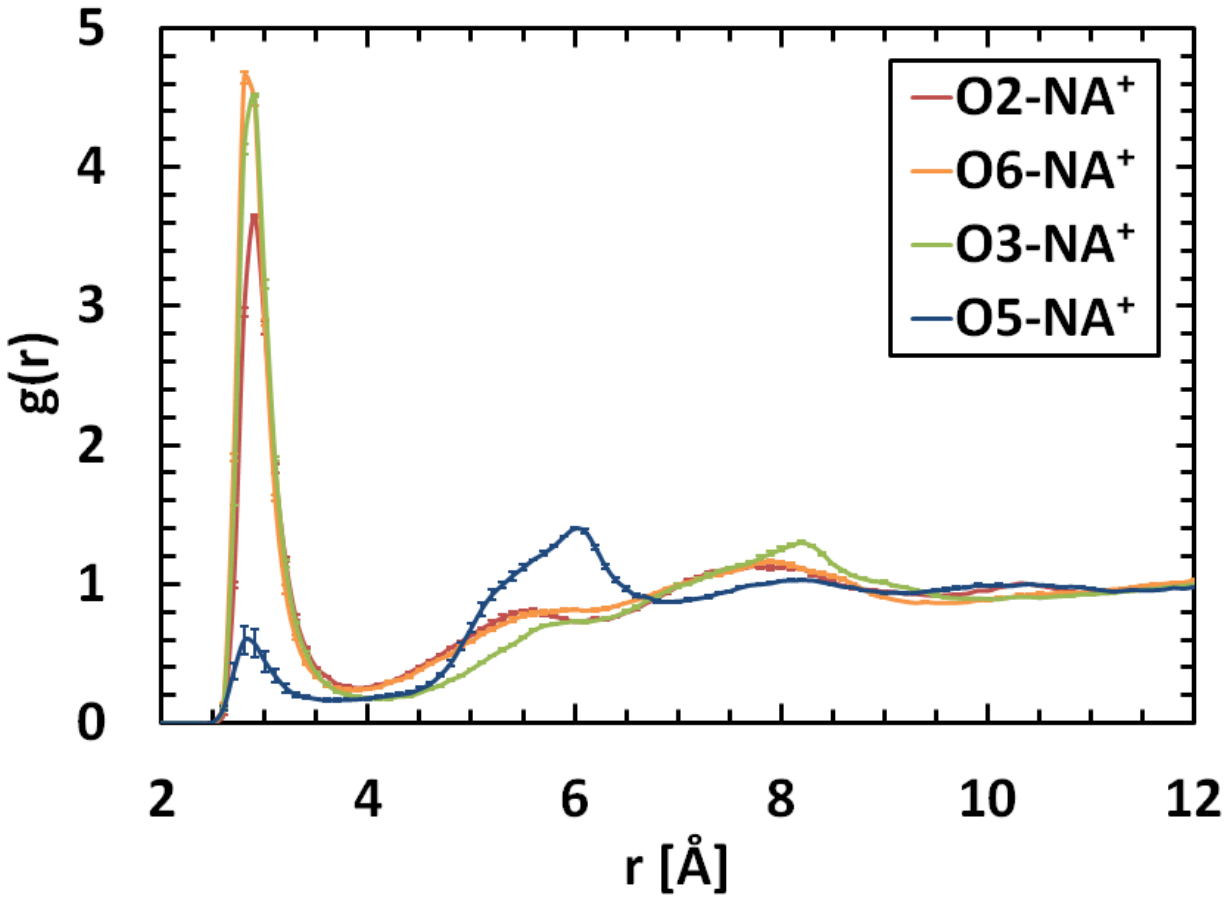

Figure S12. Radial distribution function g(r) between nitrogen atoms of each solvent-solvent pair with standard error bars. A^+ is ammonium cation, T^- is thiocyanate anion, and A is ammonia.

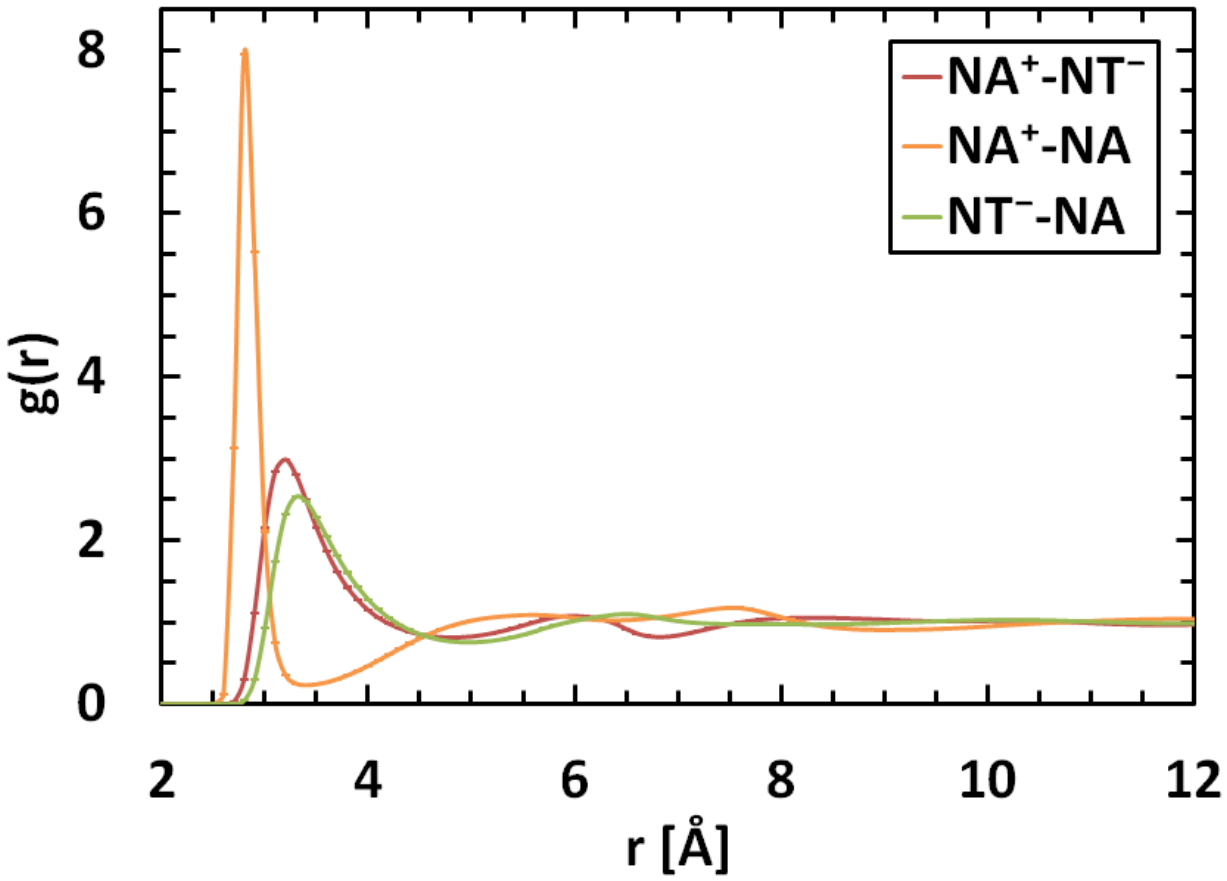

Figure S13. Impact of A:At pretreatment time (3, 6, or 24 h) on enzymatic saccharification rate, obtained for both controls (cellulose III or cellulose I) and respective A:At treated cellulose samples, at various C. Tec2 cellulase enzyme loadings ranging from 0.05-5 mg enzyme/g glucan loading. Here, (A) shows data for cellulose III while (B) shows cellulose I relevant data. All hydrolysis reactions were conducted for 24 hours and total solubilized sugar concentration in the supernatant were then quantified using standard DNS assay (using glucose as standard).

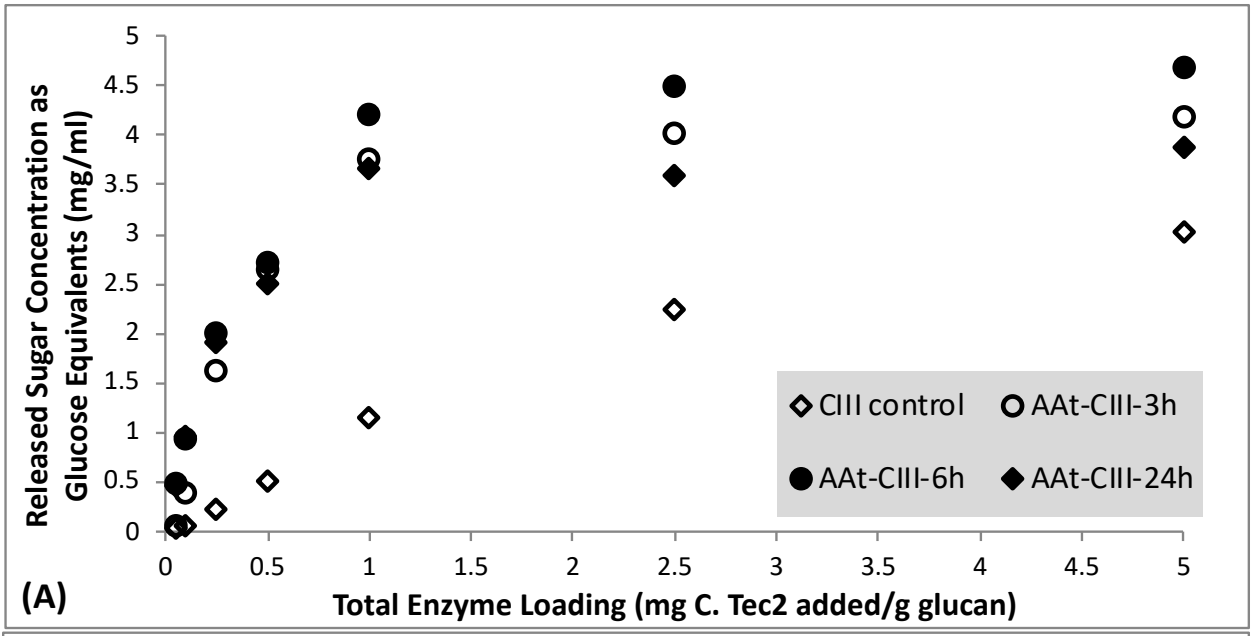

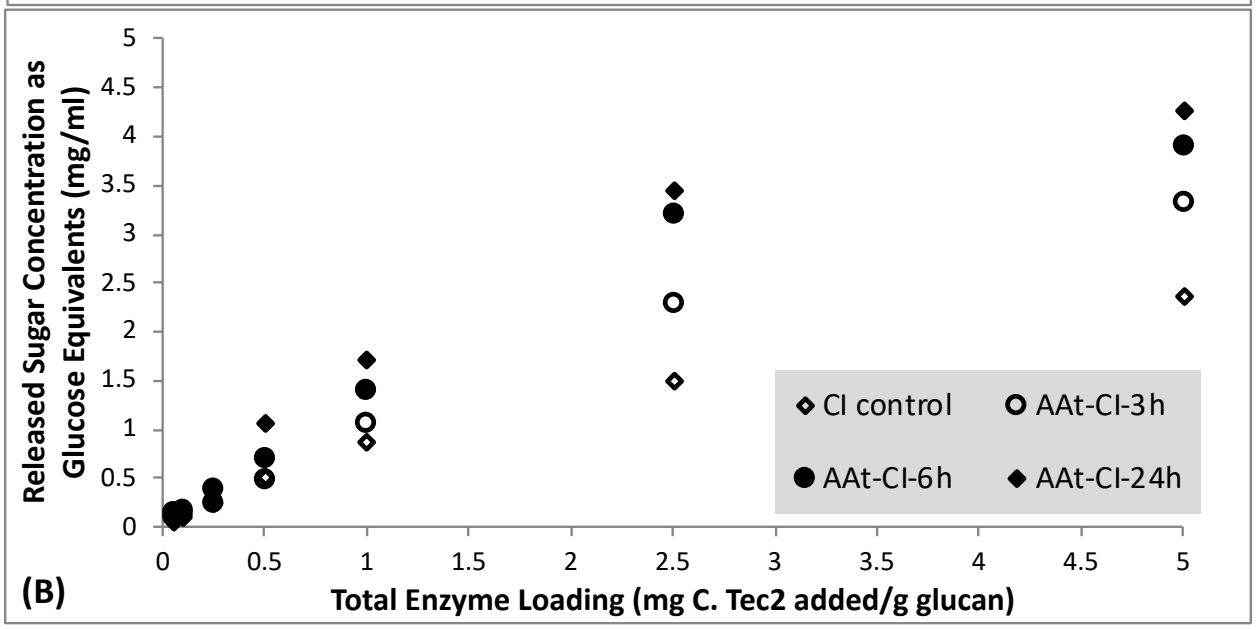

ESI Additional References

(1) Chundawat, S. P. S.; Bellesia, G.; Uppugundla, N.; Sousa, L.; Gao, D.; Cheh, A.; Agarwal, U.; Bianchetti, C.; Phillips, G.; Langan, P.; Balan, V.; Gnanakaran, S.; Dale, B. E. Restructuring the Crystalline Cellulose Hydrogen Bond Network Enhances Its Depolymerization Rate. *J. Am. Chem. Soc.* **2011**, *133* (29), 11163–11174 DOI: 10.1021/ja2011115.

(2) Park, S.; Baker, J.; Himmel, M.; Parilla, P.; Johnson, D. Cellulose Crystallinity Index: Measurement Techniques and Their Impact on Interpreting Cellulase Performance. *Biotechnol. Biofuels* **2010**, *3* (1), 10.

(3) Garvey, C. J.; Parker, I. H.; Simon, G. P. On the Interpretation of X-Ray Diffraction Powder Patterns in Terms of the Nanostructure of Cellulose I Fibres. *Macromol. Chem. Phys.* **2005**, *206* (15), 1568–1575 DOI: 10.1002/macp.200500008.

(4) Resch, M. G.; Baker, J. O.; Decker, S. R. Low Solids Enzymatic Saccharification of Lignocellulosic Biomass. *Tech. Rep. NREL/TP-5100-63351, Lab. Anal. Proced.* **2015**, No. February, 1–9 DOI: 10.1016/j.jallcom.2018.03.019.

(5) Gao, D.; Chundawat, S. P. S.; Krishnan, C.; Balan, V.; Dale, B. E. Mixture Optimization of Six Core Glycosyl Hydrolases for Maximizing Saccharification of Ammonia Fiber Expansion (AFEX) Pretreated Corn Stover. *Bioresour. Technol.* **2010**, *101* (8), 2770–2781 DOI: 10.1016/j.biortech.2009.10.056.

(6) De Groot, A. W.; Guinnup, D. E.; Thiel, M. H.; Cuculo, J. A. Light-Scattering Studies on Solutions of Cellulose in the Ammonia / Ammonium Thiocyanate Solvent System. II. Quasielastic Light-Scattering and Liquid Crystal Study. *J. Polym. Sci. Part B Polym. Phys.* **1991**, *29* (5), 557–563 DOI: 10.1002/polb.1991.090290505.

(7) Hudson, S. M.; Cuculo, J. A. The Solubility of Cellulose in Liquid Ammonia/Salt Solutions. *J. Polym. Sci. Polym. Chem. Ed.* **1980**, *18* (12), 3469–3481 DOI: 10.1002/pol.1980.170181214.

(8) Sluiter, J. B.; Ruiz, R. O.; Scarlata, C. J.; Sluiter, A. D.; Templeton, D. W. Compositional Analysis of Lignocellulosic Feedstocks. 1. Review and Description of Methods. *J. Agric. Food Chem.* **2010**, *58* (16), 9043–9053 DOI: 10.1021/jf1008023.

(9) Templeton, D. W.; Scarlata, C. J.; Sluiter, J. B.; Wolfrum, E. J. Compositional Analysis of Lignocellulosic Feedstocks. 2. Method Uncertainties. *J. Agric. Food Chem.* **2010**, *58* (16), 9054–9062 DOI: 10.1021/jf100807b.

(10) da Costa Sousa, L.; Jin, M.; Chundawat, S. P. S.; Bokade, V.; Tang, X.; Azarpira, A.; Lu, F.; Avci, U.; Humpula, J.; Uppugundla, N.; Gunawan, C.; Pattathil, S.; Cheh, A. M.; Kothari, N.; Kumar, R.; Ralph, J.; Hahn, M. G.; Wyman, C. E.; Singh, S.; Simmons, B. A.; Dale, B. E.; Balan, V. Next-Generation Ammonia Pretreatment Enhances Cellulosic Biofuel Production. *Energy Environ. Sci.* **2016**, *9*, 1215–1223 DOI: 10.1039/C5EE03051J.

(11) da Costa Sousa, L.; Foston, M.; Bokade, V.; Azarpira, A.; Lu, F.; Ragauskas, A. J.; Ralph, J.; Dale, B.; Balan, V. Isolation and Characterization of New Lignin Streams Derived from Extractive-Ammonia (EA) Pretreatment. *Green Chem.* **2016**, *18* (15), 4205–4215 DOI:

10.1039/C6GC00298F.

(12) Chundawat, S. P. S.; Donohoe, B. S.; Sousa, L.; Elder, T.; Agarwal, U. P.; Lu, F.; Ralph, J.; Himmel, M. E.; Balan, V.; Dale, B. E. Multi-Scale Visualization and Characterization of Plant Cell Wall Deconstruction during Thermochemical Pretreatment. *Energy Environ. Sci.* **2011**, *4* (3), 973–984 DOI: 10.1039/C0EE00574F.

(13) Martínez, L.; Andrade, R.; Birgin, E. G.; Martínez, J. M. PACKMOL: A Package for Building Initial Configurations for Molecular Dynamics Simulations. *J. Comput. Chem.* **2009**, *30* (13), 2157–2164 DOI: 10.1002/jcc.21224.

(14) Yu, W.; He, X.; Vanommeslaeghe, K.; MacKerell, A. D. Extension of the CHARMM General Force Field to Sulfonyl-Containing Compounds and Its Utility in Biomolecular Simulations. *J. Comput. Chem.* **2012**, *33* (31), 2451–2468 DOI: 10.1002/jcc.23067.

(15) Vanommeslaeghe, K.; Hatcher, E.; Acharya, C.; Kundu, S.; Zhong, S.; Shim, J.; Darian, E.; Guvench, O.; Lopes, P.; Vorobyov, I.; Mackerell, A. D. CHARMM General Force Field: A Force Field for Drug-like Molecules Compatible with the CHARMM All-Atom Additive Biological Force Fields. *J. Comput. Chem.* **2009**, *31* (4), NA-NA DOI: 10.1002/jcc.21367.

(16) Jorgensen, W. L.; Chandrasekhar, J.; Madura, J. D.; Impey, R. W.; Klein, M. L. Comparison of Simple Potential Functions for Simulating Liquid Water. *J. Chem. Phys.* **1983**, *79* (2), 926–935 DOI: 10.1063/1.445869.

(17) D. MacKerell, A.; Bashford, D.; Bellott, M.; L. Dunbrack, R.; D. Evanseck, J.; J. Field, M.; Fischer, S.; Gao, J.; Guo, H.; Ha, S.; Joseph-McCarthy, D.; Kuchnir, L.; Kuczera, K.; T. K. Lau, F.; Mattos, C.; Michnick, S.; Ngo, T.; T. Nguyen, D.; Prodhom, B.; E. Reiher, W.; Roux, B.; Schlenkrich, M.; C. Smith, J.; Stote, R.; Straub, J.; Watanabe, M.; Wiórkiewicz-Kuczera, J.; Yin, D.; Karplus, M. All-Atom Empirical Potential for Molecular Modeling and Dynamics Studies of Proteins. *J. Phys. Chem. B* **1998**, *102* (18), 3586–3616 DOI: 10.1021/jp973084f.

(18) Mayne, C. G.; Saam, J.; Schulten, K.; Tajkhorshid, E.; Gumbart, J. C. Rapid Parameterization of Small Molecules Using the Force Field Toolkit. *J. Comput. Chem.* **2013**, *34* (32), 2757–2770 DOI: 10.1002/jcc.23422.

(19) Humphrey, W.; Dalke, A.; Schulten, K. VMD: Visual Molecular Dynamics. *J. Mol. Graph.* **1996**, *14* (1), 33–38 DOI: 10.1016/0263-7855(96)00018-5.

(20) Frisch, M. J.; Trucks, G. W.; Schlegel, H. B.; Scuseria, G. E.; Robb, M. A.; Cheeseman, J. R.; Scalmani, G.; Barone, V.; Petersson, G. A.; Nakatsuji, H.; Li, X.; Caricato, M.; Marenich, A.; Bloino, J.; Janesko, B. G.; Gomperts, R.; Mennucci, B.; Hratchian, H. P.; Ort, J. V.; Fox, D. J. Gaussian 09, Revision E.01. Gaussian, Inc.: Wallingford CT 2013.

(21) Marcus, Y. A Simple Empirical Model Describing the Thermodynamics of Hydration of Ions of Widely Varying Charges, Sizes, and Shapes. *Biophys. Chem.* **1994**, *51* (2–3), 111–127 DOI: 10.1016/0301-4622(94)00051-4.

(22) Abraham, M. J.; Murtola, T.; Schulz, R.; Páll, S.; Smith, J. C.; Hess, B.; Lindahl, E. GROMACS: High Performance Molecular Simulations through Multi-Level Parallelism from Laptops to Supercomputers. *SoftwareX* **2015**, *1–2*, 19–25 DOI:

10.1016/J.SOFTX.2015.06.001.

(23) Foote, H. W.; Hunter, M. A. Equilibrium in the System Ammonia-Ammonium Thiocyanate. *J. Am. Chem. Soc.* **1920**, *42* (1), 69–78 DOI: 10.1021/ja01446a010.

(24) Bussi, G.; Donadio, D.; Parrinello, M. Canonical Sampling through Velocity Rescaling. *J. Chem. Phys.* **2007**, *126* (1), 014101 DOI: 10.1063/1.2408420.

(25) Berendsen, H. J. C.; Postma, J. P. M.; van Gunsteren, W. F.; DiNola, A.; Haak, J. R. Molecular Dynamics with Coupling to an External Bath. *J. Chem. Phys.* **1984**, *81* (8), 3684–3690 DOI: 10.1063/1.448118.

(26) Parrinello, M.; Rahman, A. Polymorphic Transitions in Single Crystals: A New Molecular Dynamics Method. *J. Appl. Phys.* **1981**, *52* (12), 7182–7190 DOI: 10.1063/1.328693.

(27) IIAR. *Ammonia Data Book: The Profile of a Sustainable Refrigerant Chapter Two Properties of Ammonia (by International Institute of Ammonia Refrigeration)*, 2nd Ed.; Alexandria, Virginia, 2008.

(28) Abraham, M. J.; Gready, J. E. Optimization of Parameters for Molecular Dynamics Simulation Using Smooth Particle-Mesh Ewald in GROMACS 4.5. *J. Comput. Chem.* **2011**, *32* (9), 2031–2040 DOI: 10.1002/jcc.21773.

(29) Hess*, B. P-LINCS: A Parallel Linear Constraint Solver for Molecular Simulation. **2007** DOI: 10.1021/CT700200B.

(30) Shen, T.; Langan, P.; French, A. D.; Johnson, G. P.; Gnanakaran, S. Conformational Flexibility of Soluble Cellulose Oligomers: Chain Length and Temperature Dependence. *J. Am. Chem. Soc.* **2009**, *131* (41), 14786–14794 DOI: 10.1021/ja9034158.

(31) Liu, S.-H.; Rawal, T. B.; Soliman, M.; Lee, B.; Maxwell, T.; Rajasekaran, P.; Mendis, H. C.; Labbé, N.; Santra, S.; Tetard, L.; Petridis, L. Antimicrobial Zn-Based "TSOL" for Citrus Greening Management: Insights from Spectroscopy and Molecular Simulation. *J. Agric. Food Chem.* **2019**, *67* (25), 6970–6977 DOI: 10.1021/acs.jafc.9b02466.

(32) Nishiyama, Y.; Langan, P.; Chanzy, H. Crystal Structure and Hydrogen-Bonding System in Cellulose Ib from Synchrotron X-Ray and Neutron Fiber Diffraction. *J. Am. Chem. Soc.* **2002**, *124* (31), 9074–9082 DOI: 10.1021/ja0257319.

(33) Yang, M.; Zhao, W.; Wang, S.; Yu, C.; Singh, S.; Simmons, B.; Cheng, G. Dimethyl Sulfoxide Assisted Dissolution of Cellulose in 1-Ethyl-3-Methylimidazoium Acetate: Small Angle Neutron Scattering and Rheological Studies. *Cellulose* **2019**, *26* (4), 2243–2253 DOI: 10.1007/s10570-018-2218-0.

(34) Kumar, R.; Mago, G.; Balan, V.; Wyman, C. E. Physical and Chemical Characterizations of Corn Stover and Poplar Solids Resulting from Leading Pretreatment Technologies. *Bioresour. Technol.* **2009**, *100* (17), 3948–3962.

(35) Van Loon, L. R.; Glaus, M. A. *Experimental and Theoretical Studies on Alkaline Degradation of Cellulose and Its Impact on the Sorption of Radionuclides*; Villigen and Würenlingen, 1998.

(36) Haas, D. W.; Hrutfiord, B. F.; Sarkanen, K. V. Kinetic Study on the Alkaline Degradation of Cotton Hydrocellulose. *J. Appl. Polym. Sci.* **1967**, *11* (4), 587–600 DOI: 10.1002/app.1967.070110408.

(37) Chundawat, S. P. S.; Vismeh, R.; Sharma, L.; Humpula, J.; Sousa, L.; Chambliss, C. K.; Jones, A. D.; Balan, V.; Dale, B. E. Multifaceted Characterization of Cell Wall Decomposition Products Formed during Ammonia Fiber Expansion (AFEX) and Dilute-Acid Based Pretreatments. *Biores Technol* **2010**, *101*, 8429–8438 DOI: 10.1016/j.biortech.2010.06.027.

(38) Degroot, A. W.; Carroll, F. I.; Cuculo, J. A. A 13C-NMR Spectral Study of Cellulose and Glucopyranose Dissolved in the NH3/NH4SCN Solvent System. *J. Polym. Sci. Part A Polym. Chem.* **1986**, *24* (4), 673–680 DOI: 10.1002/pola.1986.080240410.

(39) Hudson, S. M.; Cuculo, J. A.; Wadsworth, L. C. The Solubility of Cellulose in Liquid Ammonia/Ammonium Thiocyanate Solution: The Effect of Composition and Temperature on Dissolution and Solution Properties. *J. Polym. Sci. Polym. Chem. Ed.* **1983**, *21* (3), 651–670 DOI: 10.1002/pol.1983.170210302.

(40) Gericke, M.; Schlufter, K.; Liebert, T.; Heinze, T.; Budtova, T. Rheological Properties of Cellulose/Ionic Liquid Solutions: From Dilute to Concentrated States. *Biomacromolecules* **2009**, *10* (5), 1188–1194 DOI: 10.1021/bm801430x.